

www.acsami.org Research Article

Enhanced Photoluminescence of Multiple Two-Dimensional van der Waals Heterostructures Fabricated by Layer-by-Layer Oxidation of MoS₂

Sojung Kang,[‡] Yoon Seok Kim,[‡] Jae Hwan Jeong, Junyoung Kwon, Jong Hun Kim, Yeonjoon Jung, Jong Chan Kim, Bumho Kim, Sang Hyun Bae, Pinshane Y. Huang, James C. Hone, Hu Young Jeong, Jin-Woo Park, Chul-Ho Lee,^{*} and Gwan-Hyoung Lee^{*}



Cite This: ACS Appl. Mater. Interfaces 2021, 13, 1245-1252



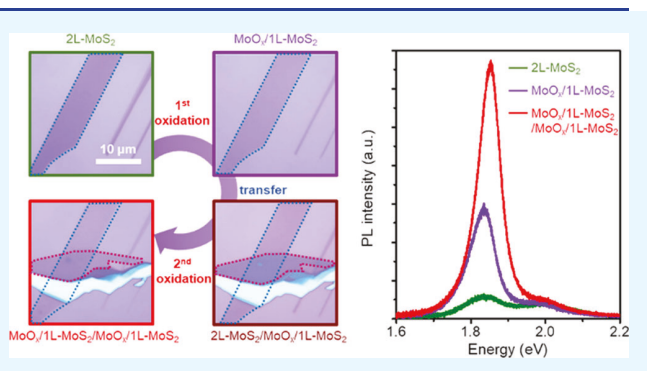
ACCESS

III Metrics & More

Article Recommendations

Supporting Information

ABSTRACT: Monolayer transition metal dichalcogenides (TMDs) are promising for optoelectronics because of their high optical quantum yield and strong light-matter interaction. In particular, the van der Waals (vdW) heterostructures consisting of monolayer TMDs sandwiched by large gap hexagonal boron nitride have shown great potential for novel optoelectronic devices. However, a complicated stacking process limits scalability and practical applications. Furthermore, even though lots of efforts, such as fabrication of vdW heterointerfaces, modification of the surface, and structural phase transition, have been devoted to preserve or modulate the properties of TMDs, high environmental sensitivity and damage-prone characteristics of TMDs make it difficult to achieve a controllable technique for surface/interface



engineering. Here, we demonstrate a novel way to fabricate multiple two-dimensional (2D) vdW heterostructures consisting of alternately stacked MoS_2 and MoO_x with enhanced photoluminescence (PL). We directly oxidized multilayer MoS_2 to a $MoO_x/1$ L- MoS_2 heterostructure with atomic layer precision through a customized oxygen plasma system. The monolayer MoS_2 covered by MoO_x showed an enhanced PL intensity 3.2 and 6.5 times higher in average than the as-exfoliated 1 L- and 2 L- MoS_2 because of preserved crystallinity and compensated dedoping by MoO_x . By using layer-by-layer oxidation and transfer processes, we fabricated the heterostructures of $MoO_x/MoS_2/MoO_x/MoS_2$, where the MoS_2 monolayers are separated by MoO_x . The heterostructures showed the multiplied PL intensity as the number of embedded MoS_2 layers increases because of suppression of the nonradiative trion formation and interlayer decoupling between stacked MoS_2 layers. Our work shows a novel way toward the fabrication of 2D material-based multiple vdW heterostructures and our layer-by-layer oxidation process is beneficial for the fabrication of high performance 2D optoelectronic devices.

KEYWORDS: molybdenum disulfide, layer-by-layer oxidation, multiple 2D van der Waals heterostructures, oxygen plasma, molybdenum oxide

■ INTRODUCTION

Transition metal dichalcogenides (TMDs), such as 2H-phase MoS₂, vary their inversion symmetry depending on the number of layers, leading to different optical and electrical properties, such as indirect-to-direct band transition and piezoelectricity of odd number of layers. Therefore, monolayer TMDs have attracted more interest than their multilayer counterparts because of strong luminescence and high quantum yield, which are useful for optoelectronic applications. To exploit the intrinsic optical properties of TMDs and confine exciton complexes in the monolayer, the van der Waals (vdW) heterostructures, such as monolayer TMD sandwiched between hexagonal boron nitride (hBN) layers, have led to efficient light emission.^{4,5} Even though stacking of the hBN as

an insulating barrier is an effective way to build vdW heterostructures of QWs, the absence of compatible oxides for TMD-based heterostructures is another obstacle toward the realization of high performance two-dimensional (2D) semiconductor devices. Therefore, a new way toward the fabrication of TMD-compatible oxide and precise layer control of TMDs is needed, similar to the case of native SiO₂ for Si. To

Received: October 13, 2020 Accepted: December 1, 2020 Published: December 23, 2020





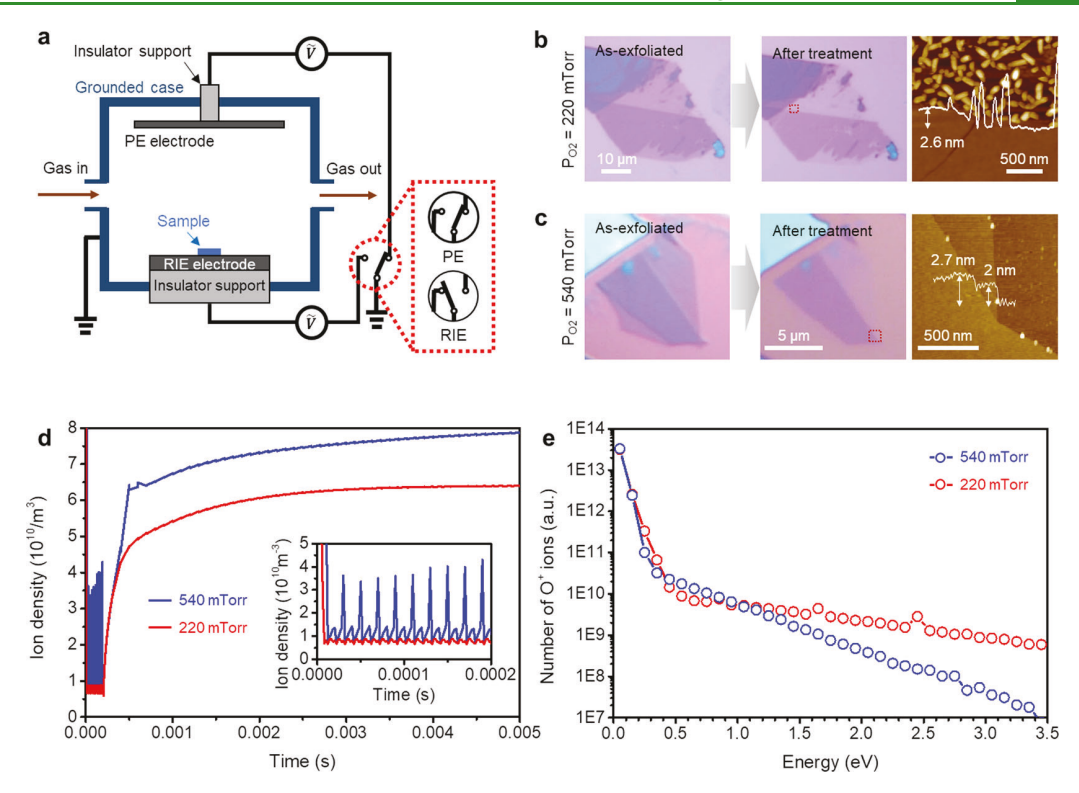


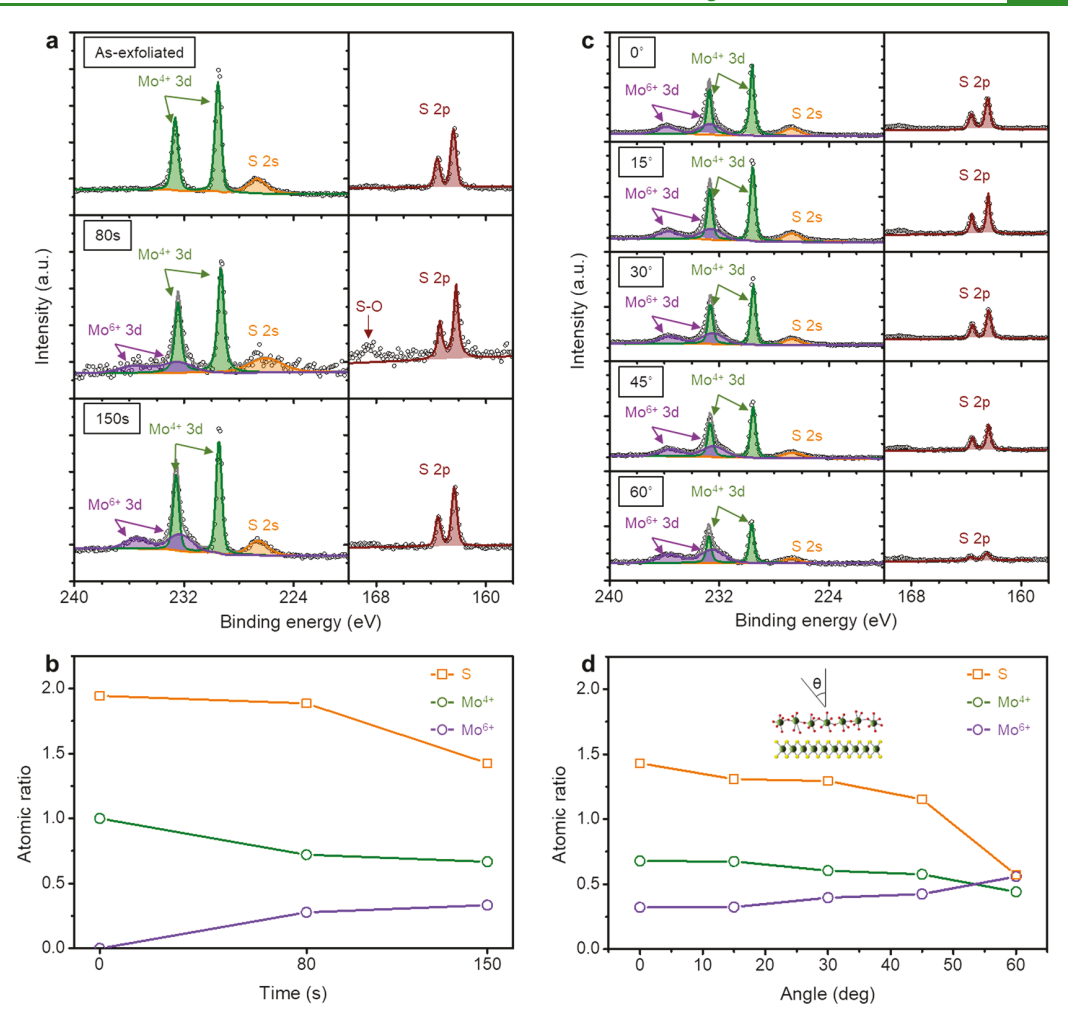
Figure 1. (a) Schematic of customized plasma equipment. (b, c) Optical and AFM images of 2 L-MoS₂ before and after oxygen plasma treatment at two different pressures of (b) 220 mTorr and (c) 540 mTorr. (d) Calculated ion density of oxygen species at different pressures. (e) Calculated energy distribution of O^+ ions at the sample position at different pressures.

convert thin TMDs into high-quality monolayers and form an oxide layer on the TMDs, various approaches, such as plasma treatment, laser thinning, annealing, and ultraviolet treatment, have been demonstrated. However, uniform oxidation and layer-by-layer thinning of bulk TMDs down to the monolayer limit without generating significant damages are still challenging because of the high etching rate and damage-prone characteristics of TMDs. 19,10

Here, we demonstrate multiple 2D vdW heterostructures of MoO_x/MoS₂/MoO_x/MoS₂, consisting of two MoS₂ monolayers separated by oxidized layers of MoO_x. For layer-by-layer oxidation of MoS₂, a customized oxygen plasma tool was developed. The topmost layers of exfoliated multilayer MoS₂ was uniformly oxidized by precisely controlled oxygen plasma treatment. This leads to the formation of MoO_x-passivated 1 L-MoS₂ with enhanced photoluminescence (PL) intensity, whose values were 3.2 and 6.5 times higher in average than the as-exfoliated 1 L- and 2 L-MoS2, respectively. This enhancement can be ascribed to the suppression of defectinduced nonradiative exciton recombination and charged exciton-related light emission in the MoO_x-covered MoS₂ layer. For the fabrication of multiple 2D vdW heterostructures, another bilayer MoS₂ was transferred onto the MoO_x/MoS₂ stack followed by a subsequent oxidation process. This heterostructure, two MoS₂ monolayers separated by ultrathin MoO_x, showed increased PL intensity as the number of stacked layers increased, reaching a higher PL intensity by 4.9 times compared to monolayer MoS₂.

■ RESULTS AND DISCUSSIONS

Oxygen plasma has been widely used to etch or oxidize TMDs. However, conventional oxygen plasma treatments are too harsh for ultrathin 2D materials, such as graphene, hBN, and TMDs, such that the 2D layers are etched away at a high rate or quickly damaged. 13 To oxidize TMDs without damage by oxygen plasma, the chemical reaction of ionized gas molecules with TMDs is preferred with minimized physical ion bombardment. ^{6,14,15} For this, we first developed a plasma tool that has two independent electrodes floating in the grounded chamber, without a coupled capacitor (Figure 1a). An AC voltage can be selectively applied to either the bottom electrode or top electrode for reactive ion etching mode or plasma etching (PE) mode, respectively, as shown in the circuit diagram in Figure 1a. The PE mode was primarily used in this work to oxidize multilayer MoS2 in a layer-by-layer manner. To optimize oxidation conditions for MoS2, we modulated several parameters of the plasma system, such as power, frequency, time, and gas pressure. The power was controlled by using the duration of driving voltage in $\pm 500~V$ square-wave. The AC voltage was applied for certain portion (4–40% for 10–100 W) of the operating time in a cycle of 5 ms. (see Supplementary Figure S1) In this work, the oxygen pressure was used as a main parameter to control the oxidation of MoS₂. For comparison, we treated the exfoliated MoS₂ at two different oxygen pressures of 220 and 540 mTorr with fixed parameters of 10 W and 50 kHz (Figure 1b,c). At a low pressure of 220 mTorr, 1 L- and 2 L-MoS₂ were etched after 150 s. The remaining cracked and scrolled regions are shown in the atomic force microscopy (AFM) image (Figure 1b) and are similar to the oxidized MoS2 under harsh oxygen plasma conditions. 11,16 Meanwhile, when a higher oxygen pressure of 540 mTorr was used, the monolayer region and topmost layer of the bilayer were uniformly oxidized, leading to a smooth surface as shown in Figure 1c. The thickness of the oxidized



www.acsami.org

Figure 2. (a) XPS of the as-exfoliated, 80 and 150 s plasma-treated MoS₂. (b) Plasma duration-dependent atomic ratio of Mo and S. (c) ARXPS of 150 s-treated MoS₂. (d) Angle-dependent atomic ratio of Mo and S.

layer measured by AFM was ~ 2 nm, which is consistent with previous reports that show the formation of 1.8 nm-thick amorphous ${\rm MoO}_x$ from plasma oxidation of monolayer ${\rm MoS}_2$.

To determine the reason for this difference, we calculated the densities of ionized oxygen at different pressures of 220 and 540 mTorr by using the finite element method (COMSOL Multiphysics). All the parameters used in the calculation, such as reaction equations, threshold energy, and rate constants, were taken from the literature. 17 When ±500 V square-wave with a fixed frequency of 50 kHz was applied, the power of the electrode was controlled by the on/off time ratio of the electrode, i.e., the electrode is on for 0.2 ms and off for 4.8 ms per 5 ms with a fixed power of 10 W. (Supplementary Figure S1) The calculated total ion densities increase up to $\sim 1 \times 10^{10}$ m^{-3} for 220 mTorr and $\sim 4 \times 10^{10}$ m⁻³ for 540 mTorr once the electrode turns on, indicating that larger oxygen pressure creates more ions (Figure 1d). However, higher oxygen pressure leads to more collisions among oxygen ions, leading to the reduction of the mean free path and average bombardment energy, as shown in Figure 1e. Therefore, the oxygen plasma treatment at higher oxygen pressure enables more precise and uniform oxidation of ultrathin MoS₂ because of the reduced bombardment effect of the oxygen ions. Hereafter, we used the optimized plasma condition (10 W, 50

kHz, 540 mTorr) for the oxidation of MoS₂. (See Supplementary Figure S2 for the effect of power and frequency on the density distribution of ions.)

To investigate compositional evolution of MoS2 during the oxidation process, X-ray photoelectron spectroscopy (XPS) was used to characterize a thick MoS2 flake exfoliated onto an Au-coated Si substrate; here, the Au was added to minimize the sample charging effect. Figure 2a shows that the asexfoliated MoS₂ has two dominant peaks of Mo⁴⁺ 3d at 229.5 and 233.6 eV as previously reported for Mo-S bonds. 18 As the plasma treatment time increased, two peaks of Mo⁶⁺ 3d emerged at 232.5 and 235.6 eV, indicating the formation of Mo-O bonds. 18 The XPS peaks of S 2p were observed at 162.3 and 163.5 eV. 19 In the plasma-treated MoS2 for 80 s, a broad peak of an intermediate state corresponding to S-O bonding appeared at 168 eV; meanwhile, it disappeared after 150 s treatment. This indicates that the sulfur atoms of the topmost layer react with oxygen in the beginning stage and are completely removed after 150 s with no remaining S-O bonds. 20,21 From the XPS results, we calculated the atomic ratio of Mo and S as shown in Figure 2b. The atomic ratios of S and Mo⁴⁺ decreased with increasing plasma treatment time because of the loss of Mo-S bonds. Meanwhile, the atom fraction of Mo6+ increased because of oxidation of MoS2 to MoO_x. To investigate depth-profile composition of oxidized

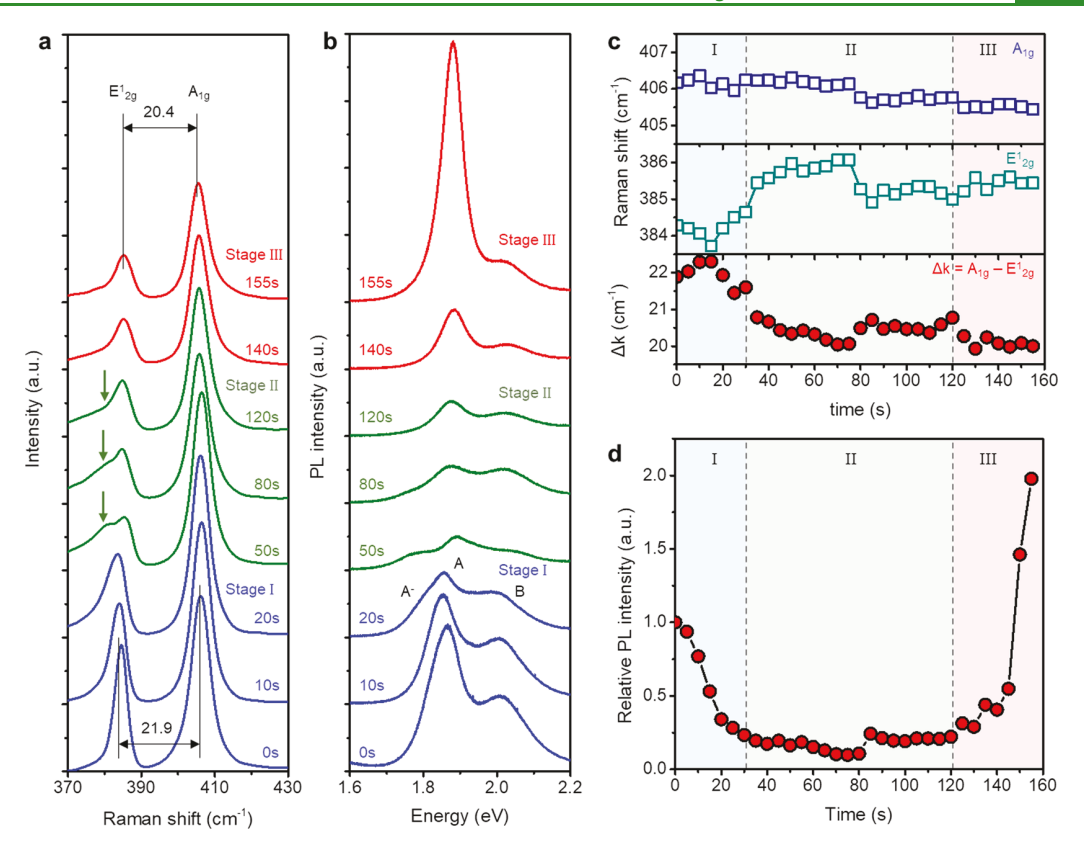


Figure 3. (a) Raman and (b) PL spectra in terms of oxygen plasma treatment duration. (c) Peak positions of A_{1g} and E_{2g}^1 vibrational mode and their difference of (d) PL intensity in height.

 ${\rm MoS}_2$, we analyzed the 150 s-treated thick ${\rm MoS}_2$ flake by using angle-resolved XPS (ARXPS) (Figure 2c). The incident angle (θ) is defined as the angle between the electron emission direction and out-of-plane direction of the sample (inset of Figure 2d). As the incident angle increased, i.e., the measured depth decreased and XPS peaks of ${\rm Mo}^{4+}$ 3d decreased, meanwhile ${\rm Mo}^{6+}$ 3d peaks increased. As shown in Figure 2d, atomic ratios of S and ${\rm Mo}^{4+}$ decreased with increasing incident angle; meanwhile the amount of ${\rm Mo}^{6+}$ increased. This result indicates that the oxidation occurs only at the topmost layer of thick ${\rm MoS}_2$ because of negligibly small bombardment energy of oxygen ions.

To systematically study the structural change and optical properties of MoS₂ during the oxidation process, we measured Raman and PL spectra of 2 L-MoS₂ during plasma oxidation (Figure 3a,b). The oxidation process can be divided into three stages as indicated with different colors in Raman and PL spectra: stage I (blue), stage II (green), and stage III (red). In stage I, the positions of two dominant Raman peaks (in-plane E_{2g}^{1} mode at 384 cm⁻¹ and out-of-plane A_{1g} mode at 406 cm⁻¹) showed no recognizable change, maintaining a frequency difference (Δk) of ~22 cm⁻¹ (Figure 3c), which is a footprint for bilayer MoS₂.²² In stage II, a significant shift of the E_{2g}^1 peak was observed with small variation of the A_{1g} peak. Note that this observation is opposite to the previous reports that the A_{1g} peak mainly downshifts because of decoupling of MoS₂ layers by O₂ intercalation.²³ Interestingly, the defectactivated peak around 380 cm⁻¹ (indicated by green arrows in Figure 3a) emerged at 50 s, then decreased as oxidation proceeded.²⁴ Raman spectra are deconvoluted into the five distinctive peaks (Supplementary Figure S3). Except for E^{1}_{2g}

and A_{1g} , we observed the longitudinal optical and transverse optical modes near E_{2g}^1 and out-of-plane optical branch near A_{1g} , which are present in the defective MoS_2 . The fact that these defect-related Raman modes disappear in stage II indicates that the partially oxidized top layer with sulfur vacancies is fully oxidized. In stage III, the frequency difference decreased to $\Delta k = 20.4~\rm cm^{-1}$ (Figure 3c), close to that of the pristine monolayer. Furthermore, the defect-activated Raman peak was not observed. This implies that the 2 L-MoS₂ was oxidized into the MoO_x -covered 1 L-MoS₂ without noticeable damage to the bottom layer from the oxygen plasma treatment.

As shown in Figure 3b,d, the PL intensity of 2 L-MoS₂ was reduced with increasing plasma treatment time in stage I and almost quenched in stage II, probably because of nonradiative recombination of excitons in the partially oxidized top layer. In stage III, the PL intensity substantially increased at 1.88 eV. Although oxygen plasma has been used for the oxidation of MoS₂ in a few papers, the bottom MoS₂ layer covered by the oxidized layer showed a significant PL quenching because of damage of the bottom layer during the oxidation process. In contrast, our results clearly show that the top layer of 2 L-MoS₂ is transformed into MoO₂, maintaining the bottom layer intact.

To explore the effect of the MoO_x layer on the electrical and optical properties of the underlying MoS_2 layer, positions of $\mathrm{E^1}_{2\mathrm{g}}$ and $\mathrm{A}_{1\mathrm{g}}$ modes are plotted as shown in Figure 4a. The red and blue arrows indicate the increasing directions of compressive strain and the p-doping level, respectively. The neutral point for strain and doping is not indicated since the as-exfoliated 1 L-MoS $_2$ generally shows different neutral points because of influences of the SiO_2 substrate and intrinsic defects as reported elsewhere. $^{26-29}$ Nevertheless, we can verify relative

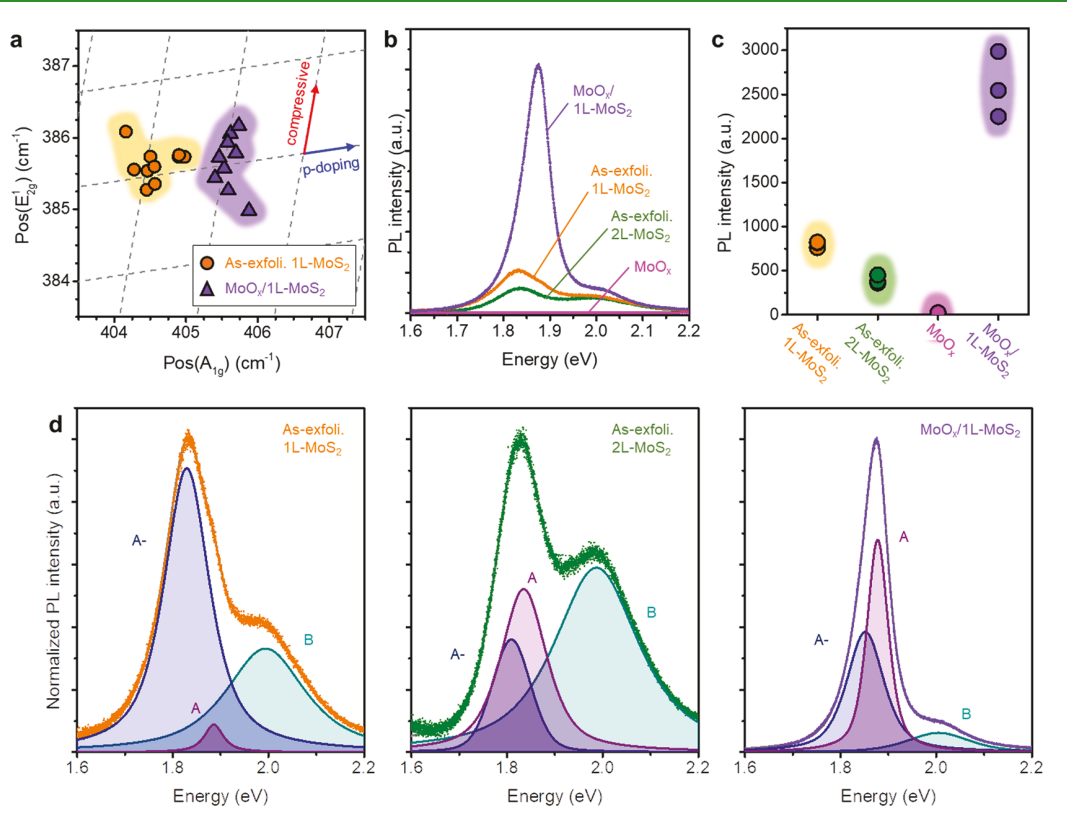


Figure 4. (a) Strain and doping comparison of the as-exfoliated 1 L-MoS₂ and MoO_x/1 L-MoS₂. (b) PL of the as-exfoliated 1 L-MoS₂, 2 L-MoS₂, MoO_x, and MoO_x/MoS₂. (c) Integrated PL intensity of the as-exfoliated 1 L-MoS₂, 2 L-MoS₂, MoO_x, and MoO_x/1 L-MoS₂. (d) Deconvolution of the as-exfoliated 1 L-, 2 L-MoS₂, and MoO_x/1 L-MoS₂.

changes of strain and doping from the shifts of two Raman peaks. It is clear that after oxidation, the strain barely changed in the $MoO_x/1$ L- MoS_2 , meanwhile the bottom MoS_2 was more p-doped than the as-exfoliated 1 L- MoS_2 , probably because of charge transfer from MoO_x . We also compared the PL spectra of the as-exfoliated 1 L- and 2 L- MoS_2 , MoO_x (oxidized from 1 L- MoS_2), and $MoO_x/1$ L- MoS_2 (oxidized from 2 L- MoS_2) in Figure 4b. The MoO_x showed no PL signal because of complete oxidation. However, the PL intensity of $MoO_x/1$ L- MoS_2 was strongly enhanced, compared to the as-exfoliated 1 L- and 2 L- MoS_2 . We summarized all PL intensities of the samples (three samples for each case) as shown in Figure 4c. The PL intensity of $MoO_x/1$ L- MoS_2 is 2.7–3.9 times and 5.0–8.3 times higher than those of the as-exfoliated 1 L- and 2 L- MoS_2 , respectively.

Such PL enhancement has been reported in oxygen plasmatreated MoS2, which was explained in terms of decoupling of layers in multilayer MoS₂ by oxygen intercalation²³ and O₂ molecule adsorption.³² However, we ruled out the first possibility in our work because no gradual enhancement of PL was observed in trilayer MoS₂ (Supplementary Figure S4) and the E12g peak upshifted with a negligible shift of A1g (Figure 3c), which are in contrast to the previous report.²³ It was reported that the second possible reason for PL enhancement, chemisorption of the O2 molecule to S vacancy sites, leads to suppression of nonradiative recombination by sulfur vacancies. 32,33 However, we observed a gradual decrease of PL in the as-exfoliated monolayer during plasma treatment. (Supplementary Figure S5). Furthermore, our low-temperature PL measurements at 4 K showed that low energy PL around 1.8 eV of the as-exfoliated 1 L-MoS₂, indicative of surface

adsorbate-related bound exciton, is quenched in the MoO_x/1 L-MoS₂ (Supplementary Figure S6).³⁴ This indicates that surface adsorption is not responsible for the PL enhancement of the MoO_x/1 L-MoS₂. A similar change of PL in the oxidized trilayer MoS₂ shows that our layer-by-layer oxidation technique can be applied to transform the thicker MoS₂ to MoO_x-coated 1 L-MoS₂ (Supplementary Figure S4). To find out the origin for the enhanced PL in $MoO_x/1$ L- MoS_2 , we deconvoluted the PL spectra of the as-exfoliated 1 L- and 2 L-MoS₂ and MoO_x/1 $L\text{-MoS}_2$ as shown in Figure 4d. Note that all PL spectra are normalized for comparison. The three main PL peaks originated from A exciton, B exciton, and A trion showed different relative intensities. The as-exfoliated 1 L-MoS₂ showed a stronger PL peak of A trion than neutral A and B excitons as it is naturally n-doped by sulfur vacancies or the substrate. $^{35-38}$ The as-exfoliated 2 L-MoS $_2$ with an indirect band structure also showed a dominant PL peak of A trion. Notably, in the MoO_x/1 L-MoS₂, the A exciton peak was enhanced with suppression of the A- trion peak. (Supplementary Figure S7) This is attributed to high dedoping of the bottom MoS₂ layer by MoO_x as aforementioned in Figure 4a. In other words, formation of trions can be restrained by eliminating a number of residual electrons in MoS₂.³⁹ Because nonradiative recombination is dominant for A- trion, generation of more neutral A exciton leads to significant PL enhancement. 40 When the trilayer MoS2 was oxidized by plasma treatment, it showed a PL spectrum similar to that of the monolayer, indicating that multilayer MoS_2 can be oxidized layer-by-layer by our oxidation process.

Finally, we fabricated a multiple 2D vdW heterostructure of MoO_x/1 L-MoS₂/MoO_x/1 L-MoS₂ by repeatedly performing

oxidation and transfer processes as shown in Figure 5a. First, the as-exfoliated 2 L-MoS₂ was oxidized into the $MoO_x/1$ L-

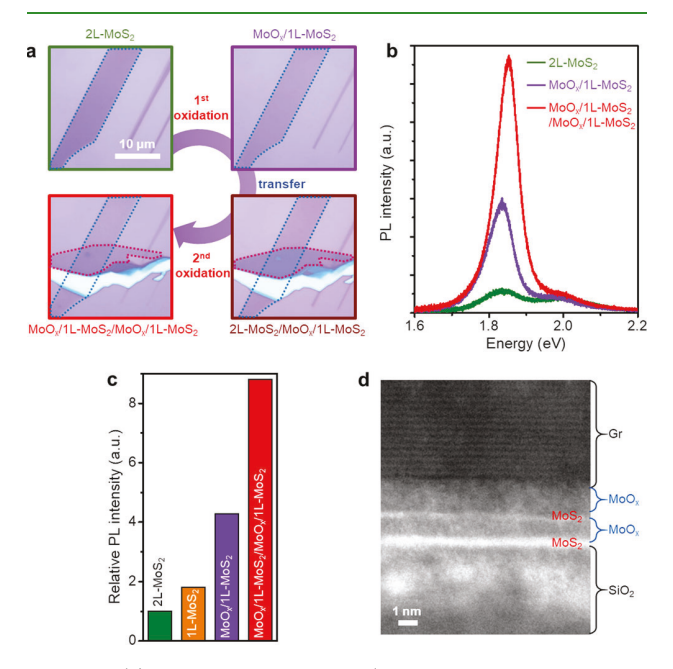


Figure 5. (a) Fabrication of AMQW ($MoO_x/1 L-MoS_2/MoO_x/1 L-MoS_2$). (b) PL of AMQW at each fabrication step. (c) PL intensity comparison of AMQW at each step and 1 L-MoS₂. (d) Dark field cross-sectional STEM image of AMQW ($MoO_x/1 L-MoS_2/MoO_x/1 L-MoS_2$).

MoS₂. Then, another as-exfoliated 2 L-MoS₂ flake was transferred onto the MoO_x/1 L-MoS₂ followed by the second oxidation. As shown in Figure 5b,c, the PL substantially increased as the layers were stacked, indicating that two lightemitting monolayers are well separated by ultrathin MoO_x in the heterostructure. The $MoO_x/1$ L- $MoS_2/MoO_x/1$ L- MoS_2 showed 2.0 and 4.8 times higher PL intensity than MoO_x/1 L-MoS₂ and 1 L-MoS₂, respectively. The multiplied PL intensity of double 2D vdW heterostructure indicates that monolayers in the heterostructure are decoupled, preventing direct-toindirect band transition of stacked MoS2 layers and carrier transport between the layers. Figure 5d shows a cross-sectional scanning transmission electron microscopy (STEM) image of the multiple 2D vdW heterostructure of MoO_x/MoS₂/MoO_x/ MoS₂, which was protected by additional top multilayer graphene during the sample preparation process. This clearly shows that the MoS₂ layers (bright) are separated by uniform MoO_x (dark). The MoO_x/MoS_2 forms a sharp heterointerface without any trapped residue.

CONCLUSIONS

In conclusion, we demonstrate a layer-by-layer oxidation method for MoS_2 using a specially designed oxygen plasma system. By optimizing the plasma condition, multilayer MoS_2 can be oxidized layer-by-layer and monolayer MoS_2 covered by MoO_x can be fabricated while maintaining the high quality of the bottom monolayer MoS_2 . The neutral exciton PL intensity of monolayer MoS_2 underneath MoO_x is remarkably enhanced because of suppression of defect-induced nonradiative recombination and charged exciton by dedoping MoS_2 by MoO_x . In the multiple 2D vdW heterostructure, the MoS_2

monolayers are well separated by uniform MoO_x layers so that multiplied PL intensity was obtained as the number of embedded MoS_2 layers increases because of suppression of the defect-induced PL quenching and interlayer decoupling. Our work suggests a novel way to fabricate the multiple 2D vdW heterostructures for advanced optoelectronic applications, which can be applied in the fabrication of high performance 2D electronic devices.

■ EXPERIMENTAL SECTION

Sample Preparation. The scotch-tape method was used for mechanical exfoliation from the MoS_2 bulk crystal (SPI Supplies Molybdenum Disulfide Crystal) onto an $SiO_2(285 \text{ nm})/Si$ substrate. For XPS, three different pieces of bulk MoS_2 were exfoliated on the Au substrate, two of which were plasma oxidized for 80 and 150 s each. The oxidation was performed ex-situ. Multiple 2D vdW heterostructures was fabricated using the PDMS dry transfer method between the two oxidation processes. For cross-sectional STEM, samples were prepared using a dual-beam focused ion beam. Few-layer graphene was transferred onto multiple 2D vdW heterostructures to minimize the damage from the C deposition followed by Pt deposition.

Plasma Treatment. Mechanically exfoliated MoS_2 was oxidized in PE mode in the plasma system (FemtoScience, CUTE); oxygen condition at a base pressure of 540 mTorr (\sim 22 sccm), 10 W, 50 kHz for 150 s for layer-by-layer oxidation. The details are described in the Supporting Information.

Finite Element Calculation. Simulation of plasma behavior and ion bombardment energy distribution to the sample surface was performed by commercial finite element method program COMSOL Multiphysics 5.3a. The details are described in Supporting Information S2.

Material Characterization. The samples were examined by AFM (Park Systems, NX-10), XPS (Kratos, Axis Supra, monochromatic Al- $K\alpha$), Raman spectroscopy and photoluminescence (Renishaw Raman, inVia Confocal Raman Microscope, 532 nm CW laser), low temperature PL (Attocube, Attodry 110, 532 nm CW laser) and cs-STEM (JEOL, JEM-ARM200F).

■ ASSOCIATED CONTENT

Supporting Information

The Supporting Information is available free of charge at https://pubs.acs.org/doi/10.1021/acsami.0c18364.

Plasma system; finite element calculation; voltage characteristics; calculated energy distribution; Raman spectra of bilayer MoS_2 after plasma treatment; PL of 3L-MoS₂; PL of 1L-MoS₂; PL of 1L-MoS₂; PL intensities of A exciton and A- trion as a function of plasma treatment duration (PDF).

AUTHOR INFORMATION

Corresponding Authors

Chul-Ho Lee — KU-KIST Graduate School of Converging Science and Technology, and Department of Integrative Energy Engineering, Korea University, Seoul 02841, Korea; Department of Integrative Energy Engineering, Korea University, Seoul 02841, Korea; Email: chlee80@ korea.ac.kr

Gwan-Hyoung Lee — Department of Materials Science and Engineering and Research Institute of Advanced Materials (RIAM), Seoul National University, Seoul 08826, Korea; Institute of Engineering Research and Institute of Applied Physics, Seoul National University, Seoul 08826, Korea; orcid.org/0000-0002-3028-867X; Email: gwanlee@snu.ac.kr

Authors

Sojung Kang – Department of Materials Science and Engineering, Yonsei University, Seoul 03722, Korea
Yoon Seok Kim – KU-KIST Graduate School of Converging Science and Technology, and Department of Integrative Energy Engineering, Korea University, Seoul 02841, Korea
Jae Hwan Jeong – Department of Materials Science and

Engineering, Yonsei University, Seoul 03722, Korea Junyoung Kwon – Department of Materials Science and Engineering, Yonsei University, Seoul 03722, Korea

Jong Hun Kim – Department of Materials Science and Engineering and Research Institute of Advanced Materials (RIAM), Seoul National University, Seoul 08826, Korea

Yeonjoon Jung – Department of Materials Science and Engineering, Seoul National University, Seoul 08826, Korea

Jong Chan Kim — Department of Materials Science and Engineering, Ulsan National Institute of Science and Technology, Ulsan 44919, Korea

Bumho Kim – Department of Mechanical Engineering, Columbia University, New York 10027, United States

Sang Hyun Bae — Department of Materials Science and Engineering, University of Illinois at Urbana—Champaign, Urbana, Illinois 61801, United States

Pinshane Y. Huang — Department of Materials Science and Engineering, University of Illinois at Urbana—Champaign, Urbana, Illinois 61801, United States; orcid.org/0000-0002-1095-1833

James C. Hone – Department of Mechanical Engineering, Columbia University, New York 10027, United States

Hu Young Jeong — UNIST Central Research Facilities and Department of Materials Science and Engineering, Ulsan National Institute of Science and Technology, Ulsan 44919, Korea; Occid.org/0000-0002-5550-5298

Jin-Woo Park — Department of Materials Science and Engineering, Yonsei University, Seoul 03722, Korea; o orcid.org/0000-0003-0965-373X

Complete contact information is available at: https://pubs.acs.org/10.1021/acsami.0c18364

Author Contributions

[‡]S.K. and Y.S.K. contributed equally. S.K., J.K., and G.-H.L. designed this work. S.K. and Y.S.K. performed all experiments including AFM, Raman spectroscopy, PL measurement, and XPS and STEM analysis. J.H.J. performed theoretical calculation for the plasma system. J.H.K. analyzed XPS data. S.K., J.C.K., and S.H.B. performed STEM measurements and analysis. B.K. performed low temperature PL measurement. All authors discussed the results. S.K., Y.S.K, G.-H.L., and C.-H.L. wrote the manuscript together. All authors have given approval to the final version of the manuscript.

Notes

The authors declare no competing financial interest.

ACKNOWLEDGMENTS

This work was supported by Korea Institute of Energy Technology Evaluation and Planning (KETEP) and the Ministry of Trade, Industry & Energy (MOTIE) of the Republic of Korea (No. 20173010013340), National Research Foundation of Korea (NRF) grant funded by the Korean government (2018M3D1A1058793, 2017R1A5A1014862, SRC program: vdWMRC center, and NRF-2020R1A2c2009389), Creative-Pioneering Researchers Pro-

gram through Seoul National University (SNU), KU-KIST school project, and NSF MRSEC award number DMR-1720633. The work was carried out in part in the Materials Research Laboratory Central Facilities at the University of Illinois. H.Y.J. acknowledges support from the Creative Materials Discovery Program through the National Research Foundation of Korea (NRF-2016M3D1A1900035).

REFERENCES

- (1) Wang, Q. H.; Kalantar-Zadeh, K.; Kis, A.; Coleman, J. N.; Strano, M. S. Electronics and Optoelectronics of Two-Dimensional Transition Metal Dichalcogenides. *Nat. Nanotechnol.* **2012**, *7*, 699–712.
- (2) Jena, D.; Banerjee, K.; Xing, G. H. 2D Crystal Semiconductors: Intimate Contacts. *Nat. Mater.* **2014**, *13*, 1076–1078.
- (3) Splendiani, A.; Sun, L.; Zhang, Y.; Li, T.; Kim, J.; Chim, C. Y.; Galli, G.; Wang, F. Emerging Photoluminescence in Monolayer MoS_2 . *Nano Lett.* **2010**, *10*, 1271–1275.
- (4) Withers, F.; Del Pozo-Zamudio, O.; Mishchenko, A.; Rooney, A. P.; Gholinia, A.; Watanabe, K.; Taniguchi, T.; Haigh, S. J.; Geim, A. K.; Tartakovskii, A. I.; Novoselov, K. S. Light-Emitting Diodes by Band-Structure Engineering in Van Der Waals Heterostructures. *Nat. Mater.* **2015**, *14*, 301–306.
- (5) Withers, F.; Del Pozo-Zamudio, O.; Schwarz, S.; Dufferwiel, S.; Walker, P. M.; Godde, T.; Rooney, A. P.; Gholinia, A.; Woods, C. R.; Blake, P.; Haigh, S. J.; Watanabe, K.; Taniguchi, T.; Aleiner, I. L.; Geim, A. K.; Fal'ko, V. I.; Tartakovskii, A. I.; Novoselov, K. S. WSe₂ Light-Emitting Tunneling Transistors with Enhanced Brightness at Room Temperature. *Nano Lett.* **2015**, *15*, 8223–8228.
- (6) Liu, Y.; Nan, H.; Wu, X.; Pan, W.; Wang, W.; Bai, J.; Zhao, W.; Sun, L.; Wang, X.; Ni, Z. Layer-by-Layer Thinning of MoS₂ by Plasma. *ACS Nano* **2013**, *7*, 4202–4209.
- (7) Sunamura, K.; Page, T. R.; Yoshida, K.; Yano, T.-a.; Hayamizu, Y. Laser-Induced Electrochemical Thinning of MoS₂. *J. Mater. Chem. C* **2016**, *4*, 3268–3273.
- (8) Lu, X.; Utama, M. I. B.; Zhang, J.; Zhao, Y.; Xiong, Q. Layer-by-Layer Thinning of MoS₂ by Thermal Annealing. *Nanoscale* **2013**, *5*, 8904–8908.
- (9) Yamamoto, M.; Einstein, T. L.; Fuhrer, M. S.; Cullen, W. G. Anisotropic Etching of Atomically Thin MoS_2 . *J. Phys. Chem. C* **2013**, 117, 25643-25649.
- (10) Liu, Y.; Tan, C.; Chou, H.; Nayak, A.; Wu, D.; Ghosh, R.; Chang, H.-Y.; Hao, Y.; Wang, X.; Kim, J.-S.; Piner, R.; Ruoff, R. S.; Akinwande, D.; Lai, K. Thermal Oxidation of WSe₂ Nanosheets Adhered on SiO₂/Si Substrates. *Nano Lett.* **2015**, *15*, 4979–4984.
- (11) Ko, T. Y.; Jeong, A.; Kim, W.; Lee, J.; Kim, Y.; Lee, J. E.; Ryu, G. H.; Park, K.; Kim, D.; Lee, Z.; Lee, M. H.; Lee, C.; Ryu, S. On-Stack Two-Dimensional Conversion of MoS₂ into MoO₃. 2D Mater. **2016**, 4, No. 014003.
- (12) Su, W.; Kumar, N.; Spencer, S. J.; Dai, N.; Roy, D. Transforming Bilayer MoS₂ into Single-Layer with Strong Photoluminescence Using Uv-Ozone Oxidation. *Nano Res.* **2015**, *8*, 3878–3886.
- (13) Kim, S.; Choi, M. S.; Qu, D.; Ra, C. H.; Liu, X.; Kim, M.; Song, Y. J.; Yoo, W. J. Effects of Plasma Treatment on Surface Properties of Ultrathin Layered MoS₂. 2D Mater. **2016**, 3, No. 035002.
- (14) Lee, G.; Lee, J.-Y.; Lee, G.-H.; Kim, J. Tuning the Thickness of Black Phosphorus Via Ion Bombardment-Free Plasma Etching for Device Performance Improvement. *J. Mater. Chem. C* **2016**, *4*, 6234–6239.
- (15) Zandiatashbar, A.; Lee, G.-H.; An, S. J.; Lee, S.; Mathew, N.; Terrones, M.; Hayashi, T.; Picu, C. R.; Hone, J.; Koratkar, N. Effect of Defects on the Intrinsic Strength and Stiffness of Graphene. *Nat. Commun.* **2014**, *5*, 3186.
- (16) Chu, X. S.; Li, D. O.; Green, A. A.; Wang, Q. H. Formation of MoO₃ and WO₃ Nanoscrolls from MoS₂ and WS₂ with Atmospheric Air Plasma. *J. Mater. Chem. C* **2017**, *5*, 11301–11309.

- (17) Turner, M. Uncertainty and Error in Complex Plasma Chemistry Models. *Plasma Sources Sci. Technol.* **2015**, *24*, No. 035027.
- (18) Zhang, X.; Jia, F.; Yang, B.; Song, S. Oxidation of Molybdenum Disulfide Sheet in Water under in Situ Atomic Force Microscopy Observation. *J. Phys. Chem. C* **2017**, *121*, 9938–9943.
- (19) Moulder, J. F.; Chastain, J., Handbook of X-Ray Photoelectron Spectroscopy: A Reference Book of Standard Spectra for Identification and Interpretation of XPS Data. Physical Electronics Division, Perkin-Elmer Corporation: 1992.
- (20) Vinoth, R.; Patil, I. M.; Pandikumar, A.; Kakade, B. A.; Huang, N. M.; Dionysios, D. D.; Neppolian, B. Synergistically Enhanced Electrocatalytic Performance of an N-Doped Graphene Quantum Dot-Decorated 3d MoS₂–Graphene Nanohybrid for Oxygen Reduction Reaction. *ACS Omega* **2016**, *1*, 971–980.
- (21) Tian, W.; Zhang, H.; Duan, X.; Sun, H.; Tade, M. O.; Ang, H. M.; Wang, S. Nitrogen- and Sulfur-Codoped Hierarchically Porous Carbon for Adsorptive and Oxidative Removal of Pharmaceutical Contaminants. ACS Appl. Mater. Interfaces 2016, 8, 7184–7193.
- (22) Liang, L.; Meunier, V. First-Principles Raman Spectra of MoS₂, Ws₂ and Their Heterostructures. *Nanoscale* **2014**, *6*, 5394–5401.
- (23) Dhall, R.; Neupane, M. R.; Wickramaratne, D.; Mecklenburg, M.; Li, Z.; Moore, C.; Lake, R. K.; Cronin, S. Direct Bandgap Transition in Many-Layer MoS₂ by Plasma-Induced Layer Decoupling. *Adv. Mater.* **2015**, *27*, 1573–1578.
- (24) Mignuzzi, S.; Pollard, A. J.; Bonini, N.; Brennan, B.; Gilmore, I. S.; Pimenta, M. A.; Richards, D.; Roy, D. Effect of Disorder on Raman Scattering of Single-Layer MoS₂. *Phys. Rev. B* **2015**, *91*, 195411.
- (25) Zhu, H.; Qin, X.; Cheng, L.; Azcatl, A.; Kim, J.; Wallace, R. M. Remote Plasma Oxidation and Atomic Layer Etching of MoS₂. ACS Appl. Mater. Interfaces **2016**, *8*, 19119–19126.
- (26) Rao, R.; Islam, A. E.; Singh, S.; Berry, R.; Kawakami, R. K.; Maruyama, B.; Katoch, J. Spectroscopic Evaluation of Charge-Transfer Doping and Strain in Graphene/MoS₂ Heterostructures. *Phys. Rev. B* **2019**, *99*, 195401.
- (27) Chae, W. H.; Cain, J. D.; Hanson, E. D.; Murthy, A. A.; Dravid, V. P. Substrate-Induced Strain and Charge Doping in Cvd-Grown Monolayer MoS₂. *Appl. Phys. Lett.* **2017**, *111*, 143106.
- (28) Michail, A.; Delikoukos, N.; Parthenios, J.; Galiotis, C.; Papagelis, K. Optical Detection of Strain and Doping Inhomogeneities in Single Layer MoS₂. *Appl. Phys. Lett.* **2016**, *108*, 173102.
- (29) Verhagen, T.; Guerra, V. L. P.; Haider, G.; Kalbac, M.; Vejpravova, J. Towards the Evaluation of Defects in MoS₂ Using Cryogenic Photoluminescence Spectroscopy. *Nanoscale* **2020**, *12*, 3019–3028.
- (30) Moody, M. J.; Henning, A.; Jurca, T.; Shang, J. Y.; Bergeron, H.; Balla, I.; Olding, J. N.; Weiss, E. A.; Hersam, M. C.; Lohr, T. L.; Marks, T. J.; Lauhon, L. J. Atomic Layer Deposition of Molybdenum Oxides with Tunable Stoichiometry Enables Controllable Doping of MoS₂. *Chem. Mater.* **2018**, *30*, 3628–3632.
- (31) Zhang, X.; Shao, Z.; Zhang, X.; He, Y.; Jie, J. Surface Charge Transfer Doping of Low-Dimensional Nanostructures toward High-Performance Nanodevices. *Adv. Mater.* **2016**, *28*, 10409–10442.
- (32) Nan, H.; Wang, Z.; Wang, W.; Liang, Z.; Lu, Y.; Chen, Q.; He, D.; Tan, P.; Miao, F.; Wang, X.; Wang, J.; Ni, Z. Strong Photoluminescence Enhancement of MoS₂ through Defect Engineering and Oxygen Bonding. *ACS Nano* **2014**, *8*, 5738–5745.
- (33) Amani, M.; Lien, D.-H.; Kiriya, D.; Xiao, J.; Azcatl, A.; Noh, J.; Madhvapathy, S. R.; Addou, R.; KC, S.; Dubey, M.; Cho, K.; Wallace, R. M.; Lee, S.-C.; He, J.-H.; Ager, J. W.; Zhang, X.; Yablonovitch, E.; Javey, A. Near-Unity Photoluminescence Quantum Yield in MoS₂. *Science* **2015**, *350*, 1065–1068.
- (34) Wang, Z. M., MoS₂: Materials, Physics, and Devices. Springer: 2016
- (35) Chee, S.-S.; Lee, W.-J.; Jo, Y.-R.; Cho, M. K.; Chun, D.; Baik, H.; Kim, B.-J.; Yoon, M.-H.; Lee, K.; Ham, M.-H. Atomic Vacancy Control and Elemental Substitution in a Monolayer Molybdenum Disulfide for High Performance Optoelectronic Device Arrays. *Adv. Funct. Mater.* **2020**, *30*, 1908147.

- (36) Mak, K. F.; He, K.; Lee, C.; Lee, G. H.; Hone, J.; Heinz, T. F.; Shan, J. Tightly Bound Trions in Monolayer MoS₂. *Nat. Mater.* **2013**, 12, 207–211.
- (37) Gogoi, P. K.; Hu, Z.; Wang, Q.; Carvalho, A.; Schmidt, D.; Yin, X.; Chang, Y.-H.; Li, L.-J.; Sow, C. H.; Neto, A. H. C.; Breese, M. B. H.; Rusydi, A.; Wee, A. T. S. Oxygen Passivation Mediated Tunability of Trion and Excitons in MoS_2 . *Phys. Rev. Lett.* **2017**, *119*, No. 077402.
- (38) Li, Y.; Qi, Z.; Liu, M.; Wang, Y.; Cheng, X.; Zhang, G.; Sheng, L. Photoluminescence of Monolayer MoS₂ on LaAlO₃ and SrTiO₃ Substrates. *Nanoscale* **2014**, *6*, 15248–15254.
- (39) Mouri, S.; Miyauchi, Y.; Matsuda, K. Tunable Photoluminescence of Monolayer MoS₂ Via Chemical Doping. *Nano Lett.* **2013**, *13*, 5944–5948.
- (40) Wei, X.; Yu, Z.; Hu, F.; Cheng, Y.; Yu, L.; Wang, X.; Xiao, M.; Wang, J.; Wang, X.; Shi, Y. Mo-O Bond Doping and Related-Defect Assisted Enhancement of Photoluminescence in Monolayer MoS₂. *AIP Adv.* **2014**, *4*, 123004.